

# TransfoRhythm: A Transformer Architecture Conductive to Blood Pressure Estimation through Solo PPG Signal Capturing

Amir Arjomand<sup>a</sup>, Amin Boudesh<sup>b</sup>, Farnoush Bayatmakou<sup>b</sup>, Georgiy Krylov<sup>a</sup>, Kenneth B. Kent<sup>a,1</sup>, Arash Mohammadi<sup>b,1</sup>

<sup>a</sup>*Faculty of Computer Science, University of New Brunswick, Fredericton, New Brunswick, Canada*

<sup>b</sup>*Concordia Institute for Information Systems Engineering, Concordia University, Montreal, Quebec, Canada*

---

## Abstract

Recent statistics indicate that approximately 1.3 billion individuals worldwide suffer from hypertension, a leading cause of premature death globally. Blood Pressure (BP) serves as a critical health indicator for accurate and timely diagnosis and/or treatment of hypertension. Traditional BP measurement methods rely on cuff-based approaches, which lack real-time, continuous, and reliable BP estimates, crucial for the timely diagnosis/treatment of hypertension. Driven by recent advancements in Artificial Intelligence (AI) and Deep Neural Networks (DNNs), there has been a surge of interest in developing data-driven and cuff-less BP estimation solutions. In this context, current literature predominantly focuses on coupling Electrocardiography (ECG) and Photoplethysmography (PPG) sensors, though this approach is constrained by reliance on multiple sensor types. An alternative, utilizing standalone PPG signals, presents challenges due to the absence of auxiliary sensors (ECG), requiring the use of morphological features while addressing motion artifacts and high-frequency noise. To address these issues, the paper introduces the TransfoRhythm framework, a Transformer-based DNN architecture built upon the recently released physiological database, MIMIC-IV. Leveraging the Multi-Head Attention (MHA) mechanism, TransfoRhythm identifies dependencies and similarities across data segments, forming a robust framework for cuff-less BP estimation solely using PPG signals. To our knowledge, this paper represents the first study to apply the MIMIC IV dataset for cuff-less BP estimation. Performance evaluation through com-

prehensive experiments demonstrates TransfoRhythm’s superiority over its state-of-the-art counterparts. Specifically, TransfoRhythm achieves highly accurate results with a Root Mean Square Error (RMSE) of [2.21, 1.84] and a Mean Absolute Error (MAE) of [1.37, 1.06] for systolic and diastolic blood pressures, respectively.

*Keywords:* Cuff-less Blood Pressure Estimation, Photoplethysmography (PPG), Transformer Neural Network, MIMIC-IV Dataset

---

## 1. Introduction

High blood pressure is a serious symptom of hypertensive disease that can lead to disability and even death [1]. Based on an estimate by the American Heart Association, approximately 41.4 % of US people will be struggling with hypertension by 2030 [2]. There are various approaches to measuring Blood Pressure, among which, cuff-based measurement [3] (where a cuff is employed to temporarily stop the blood flow to obtain the extremum BP values) is the common traditional method used both in hospitals and in-home care. Such an approach, however, carries the following drawbacks: (i) Cuff devices are not readily accessible in resource-limited settings, leading to the lack of awareness and control of hypertensive conditions; (ii) The inflation and deflation of cuffs can disrupt gold-standard hypertension diagnosis and hypotension surveillance, making these devices less suitable for frequent or prolonged usage, and; (iii) Widely used cuff-based devices fail to provide continuous BP measurement, limiting immediate detection of hypotension and real-time therapy titration [4]. Alternative methods of BP measurement, such as cuff-less monitoring, have been explored to provide continuous monitoring and reduce the potential for measurement errors caused by cuff-based methods. Cuffless BP measurement offers the potential for continuous monitoring, which enables long-term hypertension management and facilitates the precise diagnosis of cardiovascular conditions. [4]. Continuous BP monitoring offers significant advantages, particularly in detecting nocturnal BP patterns. Nocturnal BP provides critical information for the risk assessment of cardiovascular diseases (CVD). For instance, abnormally high surges or deep dips in BP during the night (more than 10 – 20%) are strongly linked to severe health outcomes, including an increased possibility of stroke, heart failure, and even mortality [5]. These fluctuations may go unnoticed with traditional cuff-based measurements, which lack the ability to continuously

track BP over time. The history of cuff-less BP estimation arises from arterial stiffness measurement through Pulse Wave Velocity (PWV) [6, 7, 8, 9]. In 1981, Geddes and Voelz tried, for the first time, to analyze Pulse Transit Time (PTT) and BP on ten dogs and reported a meaningful correlation between PTT and diastolic BP [10]. Recent cuffless measurement techniques typically employ biological signals such as Photoplethysmography (PPG), Ballistocardiography (BCG), and Electrocardiography (ECG) to estimate BP. PPG is an optical technique used to measure volumetric variations in blood circulation, offering valuable insights into the cardiovascular system. The method relies on emitting and detecting near-infrared light (wavelengths of 800–2500 nm) reflected from arterial blood flow. Changes in light absorption, caused by pulsatile blood flow through vessels, are captured by a sensor placed on the skin and can be employed for BP estimation. BCG detects body movements caused by cardiac contractions using a sensor, typically placed on a seat, which can be used for BP estimation. ECG measures the heart’s electrical activities, which can be used to derive various parameters related to cardiac function, including BP [11]. Recent advancements in machine learning (ML) have sparked a growing interest in using ML-based methods for cuff-less BP measurement from ECG and PPG signals. These ML models, particularly deep learning (DL) architectures, have demonstrated significant potential in extracting discriminative features from ECG and PPG signals, estimating blood flow volumetric changes, and predicting systolic (SBP) and diastolic (DBP) BP values. For instance, Baker *et. al* [12] developed a hybrid CNN-LSTM model using PPG and ECG signals, achieving MAEs of 4.41 mmHg for SBP and 2.91 mmHg for DBP on data from 84 subjects. Another relevant study [1] proposed a Temporal Convolutional Network (TCN) trained on the MIMIC (I, III) datasets, reporting RMSEs of 3.03 mmHg (SBP) and 1.58 mmHg (DBP). Huang *et. al* [13] introduced a modified MLP-Mixer architecture with a novel pre-processing method, achieving RMSEs of 5.10 mmHg (SBP) and 3.13 mmHg (DBP) on the MIMIC II dataset. Although BP estimation via PPG and ECG sensors is promising, it suffers from some critical drawbacks, such as reliance on two types of sensors, high power consumption, the need for sensor re-calibration, and dependence on keeping a fixed distance between sensors. A promising solution to these issues lies in using stand-alone PPG signals. Due to the ease of use and potential for BP estimation, PPG sensors have become increasingly popular in the development of advanced signal processing/learning models [14, 15, 16, 17]. In this context, when it comes to feature extraction from PPG signals, two primary approaches are employed

(as the appropriate feed for downstream processing/learning modules), i.e., raw PPG signals (time series input) [13, 18, 12, 19, 20, 21, 22, 23, 24], and feature-based vectors [25, 26, 27, 28, 29]. These representations can be extracted from the original PPG signal, multiple-order signal derivative, and Pulse Wave Decomposition (PWD) of the PPG. In the modeling step, to achieve accurate BP estimation, recent studies have employed various methodologies ranging from traditional ML models, such as Support Vector Regression (SVR) and Random Forest [29, 30, 31], to Deep Neural Network (DNN) architectures [1, 32, 21, 24] such as LSTM networks, and Gated Recurrent Unit (GRU) models with attention mechanisms [19, 28, 33, 22]. Lately, transformer-based networks have emerged as major players in this field and there are a handful of recent studies [20, 24, 34, 35, 36, 37] that investigated the potential of the attention mechanism for BP estimation through PPG signals. In summary, Nawaz et al. [37] developed an MHA model using the UCL dataset [38]. This study implemented two different models, a transformer-based architecture and a Frequency-Domain Linear/Non-linear Regression model (FD-L/NL), with the latter providing better performance. Similarly, Huang *et al.* [35] proposed a transformer-based model referred to as AriaNet, while authors in Ma *et al.* [36] focused on self-supervised transfer learning based on transformers. Furthermore, Tian *et al.* [20] proposed a CNN-Transformer model leveraging PPG signals, on the MIMIC-III dataset. Despite the advancements, standalone PPG-based BP estimation remains challenging, as removing the ECG sensor requires careful consideration of morphological features while addressing issues such as motion artifacts and high-frequency noise [39]. To address the challenges mentioned above, the paper introduces the TransfoRhythm framework, an attention-based DNN architecture built upon the recently released physiological database, MIMIC-IV dataset [40]. To our knowledge, the paper represents the first study to apply the MIMIC IV dataset for BP prediction. The TransfoRhythm framework is built on the regressive time series transformer network, which is crafted to learn from time series data while preserving sequence order and allowing parallel computation during training and inference. To expand the feature vectors' dimensionality, an embedding feature similar to those used in Natural Language Processing (NLP) tasks is employed. Positional encoding is then added to the extracted features to create the input data matrix, which is fed into a model block via the MHA mechanism. The output is refined in a position-wise block, which is then processed by a time compressor and flattening blocks to shorten the time frame and calculate estimated systolic and

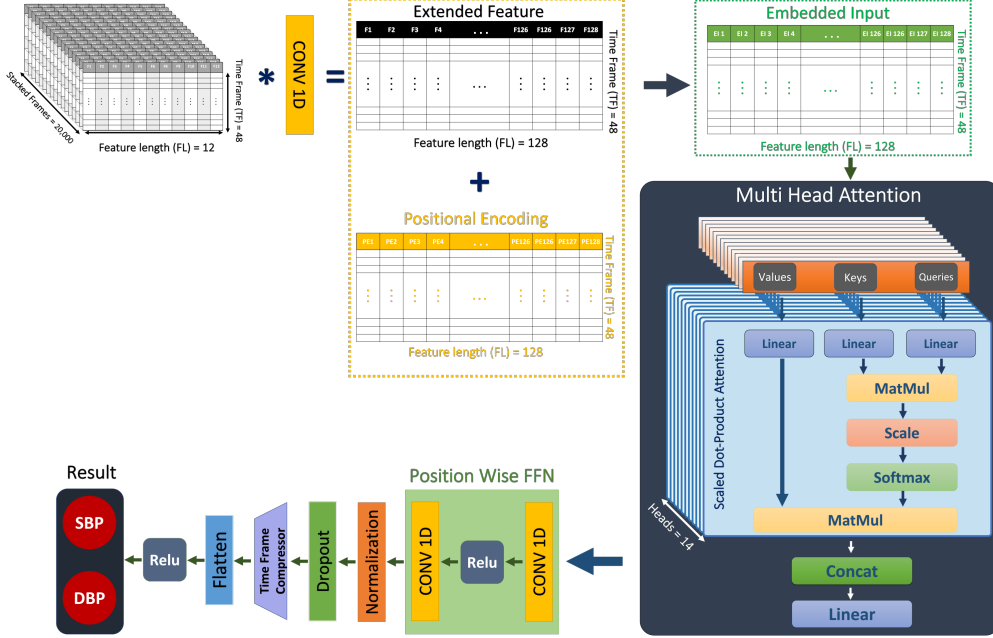


Figure 1: This block diagram depicts the streamlined process for estimating systolic and diastolic blood pressures. Features are extracted from the dataset (top left), combined with positional encoding, and form an embedded input matrix. This matrix is then inputted into the model block, which integrates a multi-head attention mechanism. The output of the model is further refined in the position-wise block. Finally, the Time compressor and flattening blocks are applied to reduce the time frame and yield the estimated systolic and diastolic blood pressure values.

diastolic BP values. The obtained results validate the effectiveness of such a modeling framework and highlight its potential for clinical implementation.

## 2. Methodology

This section focuses on material and methodology, whereas in the first part (the dataset formation subsection), we describe the preprocessing and feature extraction approaches. In the second part, the network architecture subsection provides an overview of the utilized modeling process. In summary and according to the workflow of our study, shown in Fig. 1, after dataset formation and preprocessing, the overall dataset is compiled based on 12 final features. Next, the positional encoding values are added to the flattened values of the dataset, resulting in the construction of the embedded input

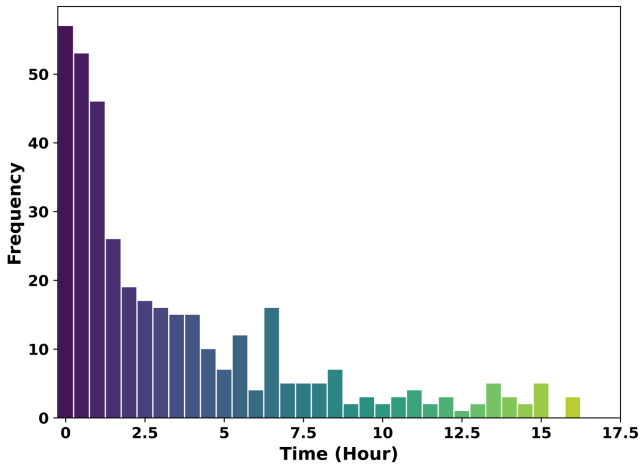


Figure 2: Time distribution of records depicted in the graph. The  $x$ -axis represents the record’s length, ranging from a few minutes to a maximum of 17 hours. The darker shades of blue indicate a higher number of observations. The majority of patients have records with a time duration of less than 1.5 hours.

matrix, which is used to feed the model. In the model part, a multi-head attention algorithm is employed. The position-wise process is applied to the output of the multi-head attention block, and finally, by reducing the time frame and flattening the position-wise output, the values related to systolic and diastolic blood pressures are obtained.

### 2.1. Dataset Formation

The Medical Information Mart for Intensive Care (MIMIC)-IV Waveform Dataset is employed, which is available on the Physio-Net repository [41] to analyze the version of waveform recordings from bedside monitoring devices in modern Intensive Care Units (ICUs). MIMIC-IV includes ECG, PPG, and invasive ABP signals and is the latest and most recently released Dataset of its kind following a joint effort from Beth Israel Deaconess Medical Center (BIDMC) and Massachusetts Institute of Technology (MIT). The recording process was conducted at a sampling rate of 62.4 Hz. All 198 individuals in the dataset were completely de-identified to ensure patient confidentiality. Fig. 2 illustrates the duration of the recorded signals and their corresponding iterations. Most patients were monitored for less than 1.5 hours, while some

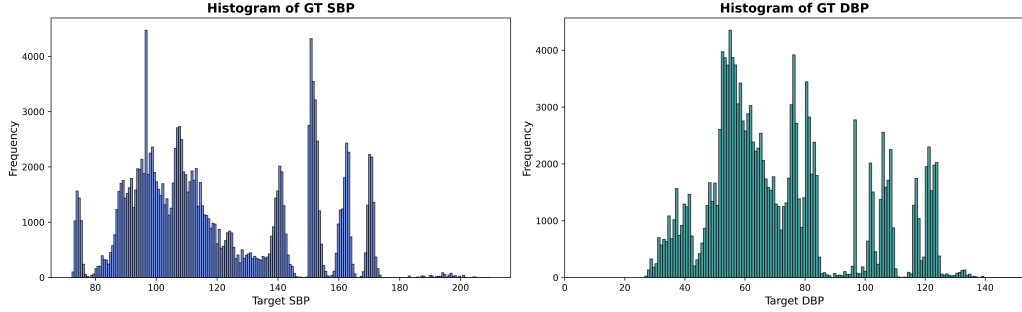


Figure 3: Distribution of patient data based on SBP and DBP values. The *x – axis* represents the blood pressure value, while the *y – axis* depicts the data frequency for systolic blood pressure (left) and diastolic blood pressure (right). Each bar corresponds to the number of records of corresponding pressure. The density of the bars reveals the concentration of observations, highlighting that most patients fall within the normal range.

patients had multiple recordings lasting over 15 hours. Although previous studies have employed MIMIC-II and MIMIC-III datasets for blood pressure estimation, to the best of our knowledge, this study stands out as the first utilization of the MIMIC-IV v2.0 dataset for this purpose.

#### 2.1.1. Preprocessing

The preprocessing stage is a crucial step in enhancing the quality of the underlying signals and removing potential noise and/or artifact sources that may have been introduced during data acquisition. In this study, in the pre-processing phase, data cleaning and signal filtering were performed. In the data cleaning step, signals with frequent out-of-range amplitudes and records that did not meet the minimum time duration (less than 15 minutes) as well as certain frames of long records that contained disqualified signals, such as flattened-line or extremely noisy segments were detected, and removed from the records. After the data cleaning step, a total of 360 purified records were identified. In the second step of the preprocessing phase, i.e., the signal filtering step, a 5<sup>th</sup> order Butterworth filter in the frequency range of 0.7 to 10 Hz and a 5<sup>th</sup> order Moving Average Filter (MAF) were applied to remove overshoots and fluctuations. More specifically, the Butterworth Infinite Impulse Response (IIR) bandpass filter was employed to remove wandering baseline and high-frequency noise, such as power-line interference (50–60 Hz). The MAF involves taking the average of a subset of data points and using it

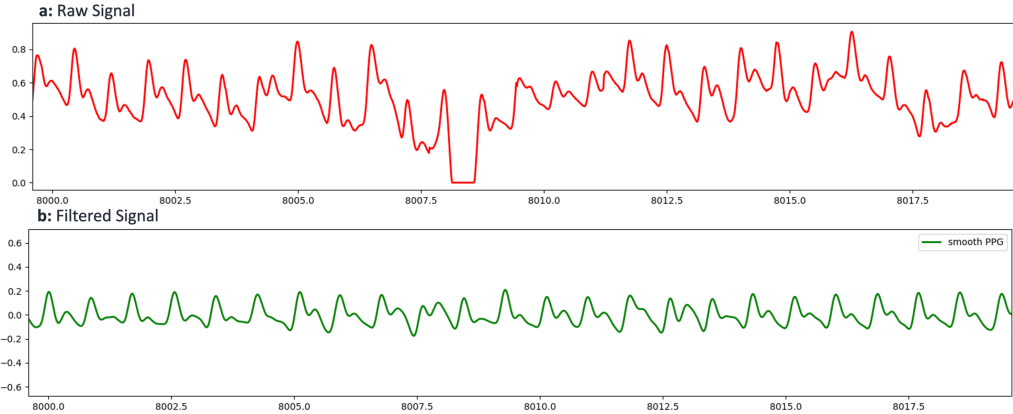


Figure 4: A comparison of the signal before and after preprocessing. The plot demonstrates the exceptional noise filtering achieved, resulting in a clean and smooth signal. Furthermore, the peaks and feet are accurately preserved, showcasing the effectiveness of the preprocessing techniques employed.

to smooth out the underlying signals. The combination of the Butterworth filter and MAF resulted in a highly filtered and smooth PPG signal. Some statistics associated with the result of the preprocessing phase are shown in Figure. 4.

### 2.1.2. Feature Extraction

For an accurate estimation of blood pressure, it is essential to focus on individual photoplethysmography (PPG) cycles. These cycles are vital for capturing important hemodynamic features such as pulse transit time (PTT), pulse amplitude, and the systolic and diastolic phases. These features, which are derived from well-defined cycles, are directly correlated with arterial stiffness and blood pressure levels. The analysis of complete 10-second frames can introduce variability and noise, which may obscure subtle physiological markers that are critical for reliable blood pressure estimation [42, 43]. The feature extraction process begins with identifying and isolating the cycles within each frame of the PPG signal. This is accomplished through a robust algorithm that simultaneously locates the peak and trough (valley) points in both the PPG signal and its second derivative (SDPPG). The algorithm is equipped with an adjustable peak-to-peak distance parameter, enabling it to effectively detect variations in peak heights and amplitudes, ultimately allowing for successful cycle extraction. Before extracting cycles,

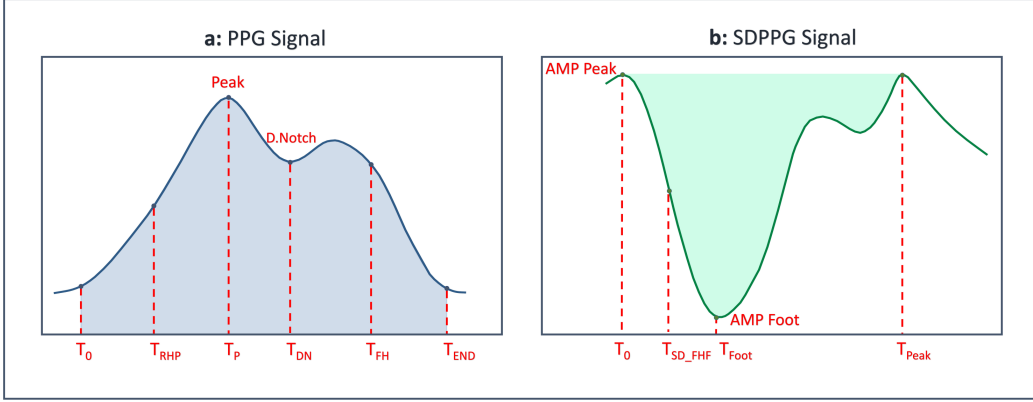


Figure 5: Characterization of features on the signal. In the PPG signal, the peak is defined as the maximum value of a PPG wave, while d.notch is defined as the minimum value between two consecutive peaks. In the SD PPG signal, amp peak refers to the maximum amplitude, while amp foot refers to the minimum amplitude between two consecutive waves.

frames are evaluated through amplitude thresholding to ensure quality by filtering out noise or artifacts caused by poor sensor contact or motion; frames with average amplitudes outside the typical PPG range are skipped. From the extracted cycles, a set of 12 features was selected based on their relationships derived from correlation analysis, with detailed descriptions provided in Table 1 and visual representations in Figure. 5.

## 2.2. Network Architecture

The proposed TransfoRhythm framework is developed based on the regressive time series transformer network, which is designed to learn from time series data while maintaining sequence order and enabling parallel computation during the training and inference phases. To enhance the dimensionality of the feature vectors, an embedding feature, previously implemented in Natural Language Processing (NLP) tasks [44] is utilized. The initial structure of the features is defined by Stacked Frames (SF) based on shuffled frames, with 20,000 frames ( $N_i$ ) and a time frame sequence of 48, which is given by

$$SF = \left[ F_T^{L,1}, F_T^{L,2}, \dots, F_T^{L,n} \right], \quad (1)$$

where  $n$  refers to the number of frames,  $F_T^{L,i}$  represents an individual frame that spans a shuffled frame with the input feature length of  $L$  ( $L_{in} = 12$ ).

Table 1: Definition of the selected features.

Feature	Symbol	Description
PPG_Cycle_Duration	TD1 = Tend - Tstart	Total Duration
PPG_Rise_Half_Peak	Trhp	The duration between the start to the half peak amplitude (rise mode)
PPG_Peak_To_Notch	TD2 = Tdn-Tp	The duration between peak to dicrotic notch
PPG_Rise_Peak	Tp	The duration between the start to the peak
PPG_Fall_Half	Tfh	The duration between peak to half of its amplitude (fall mode)
PPG_Fall_Peak	TD3 = Tend - Tp	The duration between peak to foot (end)
PPG_BPM_Frame	PBF	Cycles number per frame
PPG_Integration	PPGI = (Green Area)	Under Curve (cycle) Area
SDPPG_Fall_Half_Foot	SDPPG_Tfhf	The duration between the start to the half of its amplitude (fall mode)
SDPPG_Extremum_Amp	SDPPG_AMP	SDPPG Maximum Amplitude
SDPPG_Integration	SDPPGI = (Blue Area)	SDPPG Upper Curve Area
SDPPG_Foot_Peak	TD4 = Tpeak - Tfoot	SDPPG Duration between Foot to Peak

Furthermore,  $T$  refers to the time frame sequence and equals 48. To extract the extended features, a 1D convolution layer is applied to the stacked frames as follows

$$ST_{Extended}(N_i, L_{out}) = Bias(L_{out}) + \sum_{k=0}^{L_{in}} weight(L_{out}, k)input(N_i, k), \quad (2)$$

where  $ST_{Extended} \in \mathbb{R}^{N_i \times L_{out} \times T}$ ,  $weight \in \mathbb{R}^{L_{out} \times L_{in} \times KS}$ , and  $input \in \mathbb{R}^{N_i \times L_{in} \times T}$ . Equation. 2 expands the feature length from 12 ( $L_{in}$ ) to 128 ( $L_{out}$ ) with a kernel size ( $KS$ ) of 1.

### 2.2.1. Multi-Head Attention Mechanism

The self-attention mechanism captures the sequence dependencies and features carried on each frame. This mechanism employs three main matrices, i.e., Key, Queue, and Value, which are obtained by multiplying the input embedding matrix with learnable weights  $W_K$ ,  $W_Q$ , and  $W_V$ , respectively. The resulting matrices are then used to compute a set of attention scores. To capture additional information about in-frame sequence dependency, multiple learnable sets (Heads) are stacked and concatenated, In the current study, we utilize a multi-head attention mechanism with 14 heads for BP estimation. The architecture parameters of the networks such as heads-number are set regarding the experiments. Additionally, the model

incorporates a linear layer in the last section of multi-head attention to introduce non-linearity. This approach enables the model to capture complex relationships and dependencies among input features, resulting in better BP predictions.

Despite the self-attention mechanism being a key component of the transformer architecture, it does not incorporate information about the relative positions of tokens in the input sequence. To address this limitation, a technique called Positional Encoding (PE) was introduced that encodes the position of each element in the input sequence by adding a sinusoidal function of different frequencies to the input embedding [39]. The PE array is added, in an element-wise fashion, to the  $ST_{Extended}$  array, resulting in an Embedded input with a feature-length of 48 and a time frame sequence length of 128. The incorporated approach enables the transformer architecture to capture both the content and positional information of the input sequence.

**Position-Wise Feed-Forward Neural Network:** The next component of the attention module is the position-wise feed-forward layer that employs a 1D convolution layer with a ReLU activation function to help the model learn better representations for each position in the input sequence. This layer enables the model to capture context-specific information and understand the relationship between different positions in the sequence [45]. Furthermore, generalization techniques such as the normalization layer and dropouts are implemented to improve the model’s performance and avoid overfitting.

**Time Frame Compressor and Flattening:** In the initial stages of experimentation, we encountered computational challenges related to the extensive computational overhead on local hardware. We identified that the final flattening layer, responsible for converting the high-dimensional output into a one-dimensional structure, posed a bottleneck. To overcome this, we employed a Time Frame Compressor unit that effectively reduces dimensionality while preserving temporal signals. Specifically, this non-learnable transformer shortens the temporal order into a more condensed representation. Thereafter, in the last stage of the model, we employ a flattened layer with non-learnable weights to transform the temporally compressed signals to systolic and diastolic blood pressure values through a ReLU function.

### 2.3. Cross-Validation

To ensure robust evaluation and mitigate overfitting, we employed a 5-fold cross-validation strategy. The dataset, comprising approximately 126,000

observations, was randomly shuffled and split into five equal subsets, with each fold containing 20% of the total observations ( 25,200 records per fold). During each training iteration, 80% of the data ( 20,160 records per fold) was utilized for model training, while the remaining 20% ( 5,040 records per fold) was reserved for testing. This systematic division allowed the model to be trained and tested on diverse data subsets, enhancing its generalizability. The cross-validation process ensures that every observation is used for both training and testing, reducing the risk of overfitting and bias. By calculating the mean values of performance metrics across all five test folds, we obtained reliable and comprehensive assessments of the model’s performance. This approach provides a robust foundation for validating the proposed framework and highlights its potential for real-world implementation.

#### 2.4. Evaluation Metrics

To evaluate the effectiveness of the proposed TransfoRhythm framework, we have identified four key evaluation metrics, i.e., R-squared ( $R^2$ ), Mean Error ( $ME$ ), Mean Absolute Error ( $MAE$ ), and Root Mean Square Error ( $RMSE$ ), given by

$$R^2 = \frac{\sum_{i=1}^n (T_i - P)^2}{\sum_{i=1}^n (T_i - \bar{T})^2}, \quad (3)$$

$$ME = \frac{1}{n} \sum_{i=1}^n (T_i - P_i), \quad (4)$$

$$MAE = \frac{1}{n} \sum_{i=1}^n |T_i - P_i|, \quad (5)$$

$$RMSE = \sqrt{\frac{1}{n} \sum_{i=1}^n (T_i - P_i)^2}. \quad (6)$$

where  $T_i$  refers to the target and  $P_i$  is the predicted value. In brief, Metric  $R^2$  serves as an indicator of the extent to which the variance in the dependent variable can be attributed to the independent variables. The other metrics ( $ME$ ,  $MAE$ , and  $RMSE$ ) quantify the magnitude and/or percentage of errors between actual and predicted values.

Table 2: Values of the considered hyperparameters

Hyperparameters	Type and Value
Dropout	0.15
Optimization Algorithm	Adam
Learning Rate	1E-4 (with dynamic weight decay)
Activation Function	ReLU
Loss Function	MSE
Batch Size	128
Epoch	400

### 3. Results

To evaluate the proposed TransfoRhythm framework, comprehensive experiments were conducted by varying hyperparameters and modifying architectural components. The finalized set of hyperparameters is outlined in Table 2. Training was performed for 400 epochs on a local server equipped with an Intel 12700 CPU, 16 GB of RAM, and an Nvidia RTX 3060 GPU with 12 GB of VRAM. Performance metrics, including  $R^2$ , mean error (ME), mean absolute error (MAE), and root mean square error (RMSE), were calculated based on cross-validation results as detailed in the methodology section.

The model achieved high predictive accuracy, with mean  $R^2$  values of 0.993 and 0.994 for systolic blood pressure (SBP) and diastolic blood pressure (DBP), respectively. The mean error ranged from  $-0.31$  to  $-0.06$ , mean MAE values were 1.50 mmHg for SBP and 1.17 mmHg for DBP, and mean RMSE values were 1.84 mmHg for SBP and 1.42 mmHg for DBP. These results demonstrate that the proposed TransfoRhythm framework can reliably estimate blood pressure across different data subsets, as validated through cross-validation. Detailed performance comparisons are provided in Table 5.

#### 3.1. Error Investigation

Understanding the behavior of prediction errors and their alignment with ground truth values is essential for evaluating the reliability and robustness of the proposed TransfoRhythm framework. Figure 6 presents the distribution of errors for both systolic (SBP) and diastolic (DBP) blood pressure predictions. The histograms are centered around zero, indicating that the model's performance is well-balanced, with no significant bias toward over- or underestimation. The relatively narrow spread of errors suggests that most

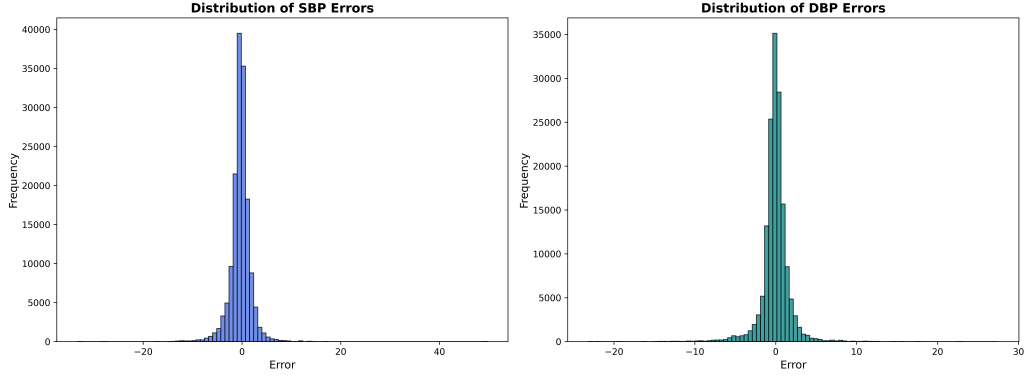


Figure 6: Distributions of prediction errors for systolic (SBP) and diastolic (DBP) blood pressure measurements. The error histograms are centered around zero, indicating balanced model performance for SBP and DBP.

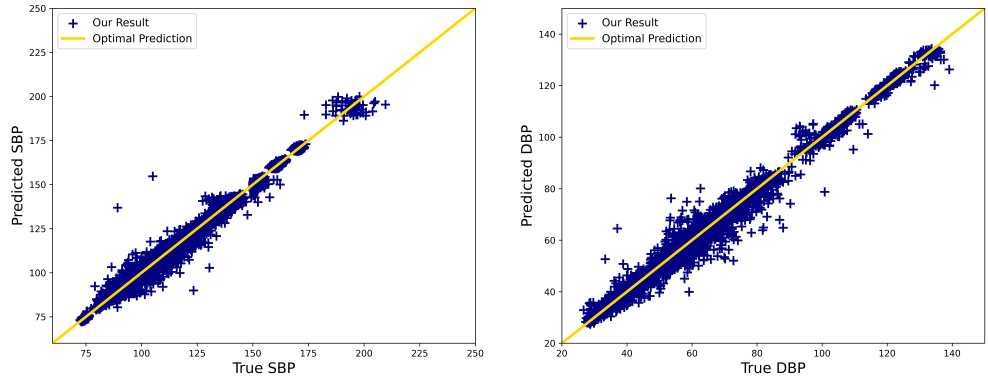


Figure 7: True versus predicted blood pressure values for systolic blood pressure (left) and diastolic blood pressure (right). The data points (navy color) indicate model predictions, while the golden line represents the ideal correspondence between true and predicted values.

predictions are in close agreement with the true values, highlighting the precision of the model. In Figure 7, the relationship between true and predicted values is shown, with the left plot representing SBP and the right plot showing DBP. Each data point reflects a model prediction, and the golden line represents the ideal one-to-one correspondence. The strong alignment of data points along this line demonstrates the model's ability to produce accurate predictions across a wide range of blood pressure values, confirming its

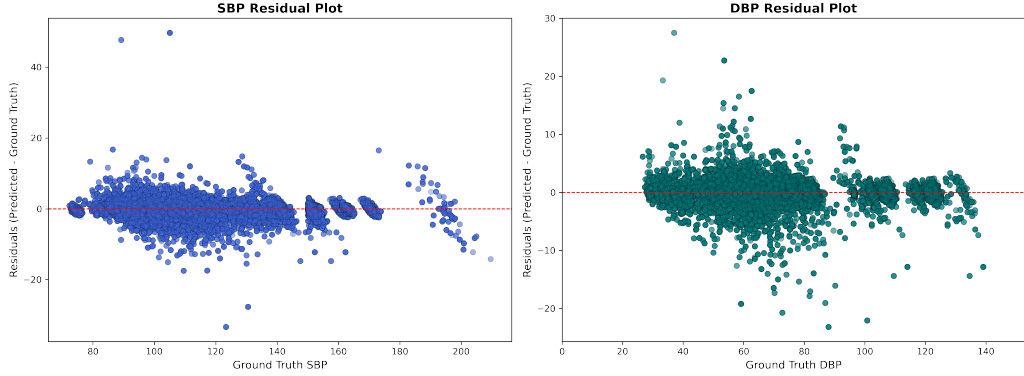


Figure 8: Residual plots for systolic (SBP) and diastolic (DBP) blood pressure predictions. The dashed red line represents zero residuals, emphasizing a balanced error distribution around this reference.

Table 3: Evaluation of the Proposed Model with AAMI and BHS Standards.

	Records	ME (mmHg)	STD (mmHg)	Cumulative error percentage		
				<5 mmHg	<10 mmHg	<15 mmHg
<b>TransfoRhythm Architecture</b>	SBP	360	0.138	1.93	96.68%	99.53%
	DBP	360	-0.166	1.58	97.40%	99.54%
<b>AAMI Standard Requirement</b>	>85	<5	<8	-	-	-
<b>BHS Standard Requirement</b>	Grade A	-	-	-	60%	85%
	Grade B	-	-	-	50%	75%
	Grade C	-	-	-	40%	65%

generalizability and robustness. Furthermore, the residual plots in Figure 8 provide additional insights by illustrating the differences between predicted and true values. The residuals are evenly distributed around a dashed red line representing zero error, indicating a lack of systematic bias. This uniform distribution of residuals emphasizes the model’s reliability and consistency in estimating both SBP and DBP across various samples. Together, these analyses underscore the effectiveness of the TransfoRhythm framework in delivering accurate and unbiased blood pressure predictions.

### 3.2. Validation against AAMI and BHS Standards

To ensure that the proposed TransfoRhythm architecture meets the international standards for medical device regulation, we evaluated our findings using the standards of the Association for the Advancement of Medical

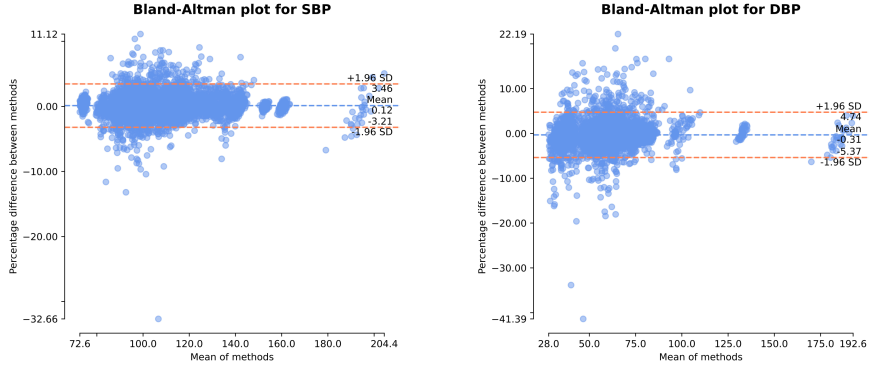


Figure 9: Bland-Altman plots for assessing agreement between ground truth and predicted values of SBP and DBP.

Instrumentation (AAMI) and The British Hypertension Society (BHS). To comply with AAMI standards, certain statistical conditions must be met, including a sample size of at least 85 individuals aged 12 years or older, a Mean Error (ME) of less than 5 mmHg, and a Standard Deviation (SD) of the error less than 8 mmHg. Additionally, BHS grades accuracy based on the cumulative percentage of error. Table 3 provides a comparison between our results and these standard metrics. As presented in Table 3 the proposed model in this study has successfully met the AAMI standard. Moreover, the model has also achieved “Grade A” in the BHS standard. These results confirm the reliability and outstanding performance of the proposed model based on the prediction error values.

### 3.3. Statistical Assessment via Bland-Altman

The Bland-Altman method is a statistical approach to evaluate the agreement between two measurement techniques by plotting their differences against their mean. This method provides a visual and quantitative assessment of bias and the range within which the two methods agree. In Figure. 9, the Bland-Altman plot for the TransfoRhythm model demonstrates a mean difference of 0.26 mmHg for SBP, with 95% limits of agreement ranging from  $-3.60$  mmHg to  $4.12$  mmHg. For DBP, the mean difference is  $0.07$  mmHg, with 95% limits of agreement spanning  $-5.81$  mmHg to  $5.96$  mmHg. These results indicate that the TransfoRhythm model has minimal systematic bias and maintains a relatively narrow range of agreement. Additionally, the

random distribution of differences around the mean suggests the absence of proportional bias, highlighting the model’s reliability. This analysis confirms the potential of the TransfoRhythm model for accurate and consistent blood pressure estimation in clinical applications.

### *3.4. Comparisons with Benchmark Models*

This section focuses on validating our results by comparing the performance of our proposed model with benchmark algorithms from previous studies. Given the lack of prior work utilizing the MIMIC IV dataset for BP prediction, we implemented benchmark models from other studies that analyzed earlier versions of the MIMIC dataset. These benchmark models are employed to establish a baseline performance for blood pressure estimation in the context of the MIMIC IV dataset. The selection of benchmark models was based on specific criteria. Firstly, we considered models that exclusively utilized PPG signals. Furthermore, due to the impracticality of conducting extensive feature engineering for each model, we specifically chose models that were trained on raw data. Additionally, we selected models with open-access codes with satisfying results in their respective papers. The benchmark models enclosed various architecture families. From CNN-based networks, we selected ResNet1D and AlexNet1D, which were originally implemented and evaluated on MIMIC II and MIMIC-III datasets [46]. Additionally, we included a U-Net model that had been evaluated on the MIMIC III dataset [47]. In terms of Recurrent Neural Networks (RNN), we defined a BiLSTM model for our benchmark set, which aimed to address the absence of suitable RNN-based models meeting our selection criteria. The BiLSTM model begins with a 1D Convolutional layer for feature extraction, followed by a Max pooling layer to enhance pattern detection. Four Bidirectional LSTM layers then capture contextual understanding by considering past and future states. To prevent overfitting, four Dropout layers are placed after the LSTM layers. Finally, two dense layers are used to perform the final regression task and map features to the desired output format. By containing the BiLSTM model, we aimed to gain insights into RNN-based approaches for blood pressure prediction and expand the scope of evaluation by comparing our model performance with other benchmark models. Lastly, we incorporated a hybrid architecture combining CNN and RNN layers, which utilized the raw PPG signal along with its first and second derivatives of the MIMIC III dataset as input features [48]. It is essential to note that the pre-processing methods employed in the benchmark studies were customized for their specific MIMIC

Table 4: Comparison of the proposed model with benchmark models on Mimic IV dataset

Architecture Type	Model	MAE	MAE	RMSE	RMSE
		SBP	DBP	SBP	DBP
CNN	ResNet_1D	2.28	1.06	5.55	3.21
	AlexNet_1D	3.09	1.59	7.98	4.60
	U-Net	2.76	1.56	7.47	4.70
RNN	Bi-LSTM	3.86	1.9	7.98	4.19
Hybrid	CNN-RNN Network	2.79	1.96	5.62	3.91
<b>MHA</b>	<b>TransfoRhythm</b>	<b>1.37</b>	<b>1.06</b>	<b>2.21</b>	<b>1.84</b>

dataset version. As the structure of the MIMIC IV dataset differs from the earlier versions, we utilized our pre-processing pipelines. Additionally, since the referenced studies employed a *10 – second* window size, we maintained consistency by adopting the same window length for the data.

Table 4 presents the quantitative evaluation metrics obtained by implementing the benchmark models on the MIMIC IV dataset. Each benchmark model was trained using different sets of hyperparameters, and the most accurate model was identified and reported. The results demonstrate the superior performance of our proposed model compared to the benchmark algorithms across all the evaluation metrics. This notable performance confirms the efficacy of our approach in accurately estimating blood pressure solely from PPG signals.

#### 4. Discussion and Conclusion

Long-term BP measurement could not be carried out using cuff-based solutions because of its indiscrete nature and the inaccuracy caused by factors such as the cuff size, placement, and the patient’s movement. Consequently, there has been a surge of recent interest in using DL techniques to estimate BP based on ECG and/or PPG data [49]. In this context, the TransfoRhythm framework is developed in this study for continuous BP estimation. The TransfoRhythm takes as input 12 features extracted from the MIMIC IV raw and derivatives PPG waveforms. It is worth noting that despite many studies on the MIMIC datasets, to the best of our knowledge, this work is the first investigation of BP prediction implemented on the MIMIC IV waveform version dataset. At the core of the TransfoRhythm framework is a Multi-Head Attention (MHA)-based mechanism, which is a neural net-

work architecture with several advantages over its traditional DL methods for time series analysis [50]. Several studies have shown that MHA can outperform conventional DL methods in various time series prediction tasks. For example, MHA-based networks have been shown to outperform RNNs in predicting fault diagnosis [51], energy consumption assessment [52], and speech enhancement [53]. Additionally, MHA has been shown to improve prediction accuracy in stock price prediction [54], and traffic flow prediction [55]. When it comes to BP estimation, conventional DL methods are typically developed based on RNN and/or CNN architectures. While these methods have shown promising results, they have limitations, such as difficulty in capturing long-term dependencies or invariance to temporal shifts in the input [56] [53]. The primary advantage of MHA is its ability to attend to various input sequence segments, enabling the model to learn complicated relationships between various observations in the sequence and improve representations of the input. It, therefore, can capture both short-term and long-term dependencies in time series data, where detailed relations between distinct observations might be difficult to capture by conventional DL methods [57] [58]. Attention-based networks have also the potential to enhance forecasting accuracy and improve the robustness of time series analysis by handling noise and perturbations [58]. Another merit of the MHA is its ability to handle variable-length inputs without using reduction methods, making it possible to learn more accurate representations of the input. In conventional DL methods, padding or truncation is often used to ensure all input sequences have the same length. This could lead to information loss and reduced model performance [52]. Finally, the Attention mechanism can also be used to improve the interpretability of the model in diverse academic contexts [59]. Attention scores can provide insight into the specific segments of the input sequence that the model focuses on when making predictions [60]. This can be extremely practical in BP studies, in which identifying important observations can provide valuable insight.

Our results, evaluated across multiple criteria, demonstrate the superiority of the proposed TransfoRhythm framework for BP estimation. The model achieved MAE and STD values in the range of [1.50, 1.84] mmHg for DBP and [1.17, 1.42] mmHg for SBP, fully meeting the AAMI and BHS standard requirements. The consistently low MAE and RMSE values highlight the model’s potential for accurate and reliable BP estimation in real-world applications. To further validate the performance of the proposed TransfoRhythm framework, we conducted two assessment stages.

Table 5: Comparison of studies in BP estimation in terms of methodology, database, features, and metrics (NR means not reported).

Model Architecture	Signal	Datasets	Input Type	MAE SBP	MAE DBP	RMSE SBP	RMSE DBP	STD SBP	STD DBP	ME SBP	ME DBP
MLPstm-BP [13]	ECG PPG	MIMIC II	Raw Waveform	3.52	2.13	5.1	3.13	5.09	3.07	0.071	-0.495
Temporal Convolution Network (TCN) [1]	ECG PPG	MIMIC I MIMIC III	Feature Extraction	2.59	1.33	3.03	1.58	3.58	1.97	-2.98	-3.65
CNN + LSTM [12]	ECG PPG	MIMIC III	Raw Waveform	4.41	2.91	NR	NR	6.11	4.23	NR	NR
NABNet (BiConvLSTM) [19]	ECG PPG	MIMIC III	Raw Waveform (multi-channel)	2.63	1.09	NR	NR	2.96	1.05	-0.678	-0.342
Bi-LSTM [61]	ECG PPG	MIMIC II	Feature Extraction	2.51	1.38	3.22	1.78	NR	NR	-0.09	-0.07
LSTM network [22]	ECG PPG	MIMIC III	Raw Waveform	8.34	3.47	NA	NA	10.68	4.76	NA	NA
Deep Autoencoder [18]	PPG	MIMIC II	Raw Waveform	5.42	3.14	NR	NR	6.64	3.74	1.65	-1.28
1D_CNN + 2D_CNN [49]	PPG	MIMIC II	Raw Waveform + Image	3.05	1.58	NR	NR	5.26	2.6	-0.15	-0.29
CNN (Transfer Learning) [39]	PPG	MIMIC II	Image (Transformed PPG)	6.17	3.66	8.46	5.36	8.46	5.36	0.00	-0.04
Bi-GRU +GRU+attention [33]	PPG	MIMIC II	Feature Extraction (22 features)	2.58	1.26	NR	NR	3.35	1.63	-0.52	-0.66
BiLSTM + LSTM + Attention [28]	PPG	MIMIC II	Feature Extraction	4.51	2.6	NR	NR	7.81	4.41	-0.48	-0.49
GRU [26]	PPG	MIMIC II	Feature Extraction (7 features)	3.25	1.43	NR	NR	4.76	1.77	NR	NR
DNN [27]	PPG	MIMIC II	Feature Extraction (32 features)	3.21	2.23	4.64	3.3	NR	NR	NR	NR
U-Net [47]	PPG	MIMIC III	Raw Waveform	5.73	3.45	NR	NR	9.16	6.14	-1.582	1.619
Feed Forward ANN [62]	PPG	MIMIC II UCI	Feature Extraction (21 features)	7.41	3.32	NR	NR	10.40	4.89	-4.02	-0.31
CNN+LSTM [63]	PPG	MIMIC III	Feature Extraction	3.79	2.89	NR	NR	7.89	5.34	0.13	0.48
ArterialNet Transformer [35]	PPG	MIMIC III	Raw waveform	4.15	3.17	5.26	4.01	1.32	1.37	NR	NR
KD-Informer [34]	PPG	MIMIC II	Backward elimination feature selection	4.00	2.97	NR	NR	5.93	3.87	0.018	0.010
MLM-Transformer w/personalization [64]	PPG	MIMIC III	Raw waveform	2.41	1.31	NR	NR	2.72	1.77	0.037	0.029
Transformer network [37]	PPG	UCI	Raw waveform	3.77	2.69	NR	NR	NR	NR	NR	NR
Self-supervised transformer (STP) [36]	PPG	MIMIC III	Raw waveform	3.37	2.48	NR	NR	4.21	2.76	0.85	0.49
U-Net + multiRes[21]	PPG	UCI	Raw Waveform	2.85	1.79	NR	NR	NR	NR	-0.89	1.06
CNN + Transformer[20]	PPG	MIMIC-III	Raw Waveform	4.44	2.36	NR	NR	5.98	3.22	0.17	0.18
TCN + Attention[24]	PPG	UCI	Raw Waveform (Derivatives)	5.3	2.11	NR	NR	8.3	3.17	NR	NR
<b>TransfoRhythm</b>	<b>PPG</b>	<b>MIMIC IV</b>	<b>Feature Extraction</b>	<b>1.37</b>	<b>1.06</b>	<b>2.21</b>	<b>1.84</b>	<b>2.21</b>	<b>1.84</b>	<b>-0.31</b>	<b>-0.06</b>

- **Benchmarks on the MIMIC IV Dataset:** In the first stage, the proposed model’s performance on the MIMIC IV dataset was compared against benchmark models trained on the same dataset, as summarized in Table 4. This comparative analysis ensures a fair evaluation and reinforces confidence in the model’s accuracy and reliability. The proposed TransfoRhythm outperforms all benchmark models, a result largely attributed to its internal MHA mechanism. By selectively attending to critical features, the MHA mechanism enables TransfoRhythm to effectively capture temporal dependencies and spatial relationships within PPG signals, enhancing its ability to focus on informative patterns for precise BP estimation. Among the benchmark models, the ResNet1D architecture demonstrated the second-best performance. ResNet1D, a variant of the Residual Neural Network, employs one-dimensional convolutional layers and residual connections to efficiently extract spatial features while addressing the vanishing gradient problem during training. Following ResNet1D, the hybrid model [48] and the U-Net [47] architecture achieved competitive results. The hybrid model leverages both CNN and RNN architectures to capture spatial and temporal dependencies, while U-Net’s modified structure is adept at extracting meaningful features from sequential data. AlexNet1D also performed well, albeit slightly behind ResNet1D and the hybrid model. AlexNet1D uses 1D convolutional layers for feature extraction followed by fully connected layers. Additionally, the Bi-LSTM model, which processes input sequences bidirectionally to encode both past and future temporal information, delivered reasonable performance. However, it fell short compared to TransfoRhythm, ResNet1D, the hybrid model, U-Net, and AlexNet1D.
- **Comparisons with the State-of-The-Art Models:** In the second stage of performance evaluation, the model’s functionality is investigated by comparing it to related state-of-the-art studies. Table 5 illustrates the comparisons, which include model architecture, input signal type, dataset, feature injection model, and metrics. The main objective is to provide a comprehensive evaluation of the model’s performance, independent of dataset consideration. This analysis allows for a thorough assessment of the model’s functionality and its relative standing compared to other advanced approaches in the field of BP estimation. Regarding datasets, most of the similar works employed MIMIC II or

MIMIC III datasets. MIMIC-IV, which was used in this study in comparison with other available MIMIC datasets, includes more PPG data. Meanwhile, MIMIC-IV includes more recent data, which may be more representative of current clinical practices, and has undergone rigorous quality control processes to ensure that the data is accurate and reliable [41]. In terms of modeling approaches, several related works have applied traditional machine learning (ML) methods, including Support Vector Machines (SVM)[65], Random Forest (RF)[66], and XG-Boost [67]. While these approaches have achieved acceptable results in specific scenarios, they were not included in Table 5 due to the superior performance of deep learning (DL) methods on time-series data such as ECG and PPG signals. Among DL approaches, studies like [39] have demonstrated the efficacy of CNNs without incorporating RNN layers for BP estimation. Other works have employed RNNs, particularly Long Short-Term Memory (LSTM) and Gated Recurrent Unit (GRU) networks, to extract temporal features from time-series data, as seen in studies like [26]. The importance of employing hybrid networks to extract temporal and recursive features of the signal was indicated by multiple studies [33, 28, 31]. For instance, Malayeri *et al.* used a hybrid CNN-based network and gathered the recursive features of the signal with a 2D CNN structure instead of RNN networks [49]. Likewise, a combination of RNN and attention layers was presented by [33, 28], and the importance of attention usage was shown. Recently, transformer-based approaches have gained prominence in BP estimation due to their ability to model long-range dependencies in time-series data. For instance, ArterialNet [35] and MLM-Transformer [64] achieved remarkable accuracy by leveraging transformer architectures with raw waveform inputs. Similarly, methods such as Self-Supervised Transformer (STP)[36] and CNN+Transformer hybrids [20] have demonstrated the growing impact of transformers in this domain. These studies emphasize the versatility and effectiveness of transformer-based models for analyzing time-series PPG data, highlighting their potential for advancing BP estimation techniques.

Despite the strong performance of the proposed TransfoRhythm framework, several limitations and future research opportunities exist. The MIMIC-IV dataset was used exclusively for training and validation, and all findings are based on this dataset. Thus, this study represents the first attempt to

develop a BP estimation model solely based on PPG signals from MIMIC-IV. Future work could investigate the model’s performance on additional datasets or incorporate diverse data sources to improve generalization. Finally, exploring more advanced attention-based network architectures could further enhance model accuracy and robustness.

### **Acknowledgments**

This Project was partially supported by the Natural Sciences and Engineering Research Council (NSERC) of Canada through the NSERC Discovery Grant RGPN-2023-05654 and RGPN-262177-12.

### **Data Availability**

The utilized dataset (Reference [41]) is publicly available through the following link: <https://www.ncbi.nlm.nih.gov/pmc/articles/PMC9780032/>

### **Author Contributions Statement**

**Amir Arjomand and Amin Boudesh:** Conceptualization, Methodology, Software, Investigation, Data curation, Validation, Visualization, Writing – original draft.

**Farnoush Bayatmakou:** Formal analysis, Resources, Writing – review and editing.

**Georgiy Krylov:** review and editing.

**Kenneth B. Kent:** Supervision, Project administration, Writing – review and editing.

**Arash Mohammadi:** Supervision, Project administration, Conceptualization, Methodology, Writing – review and editing.

### **Additional Information**

**Competing Interests:** Authors declare no competing interests.

### **References**

- [1] S. Zabihi, E. Rahimian, F. Maresfat, A. Asif, P. Mohseni, A. Mohammadi, Bp-net: Cuff-less and non-invasive blood pressure estimation via a generic deep convolutional architecture, *Biomedical Signal Processing and Control* 78 (2022) 103850.

- [2] P. A. Heidenreich, J. G. Trogdon, O. A. Khavjou, J. Butler, K. Dracup, M. D. Ezekowitz, E. A. Finkelstein, Y. Hong, S. C. Johnston, A. Khera, et al., Forecasting the future of cardiovascular disease in the united states: a policy statement from the american heart association, *Circulation* 123 (8) (2011) 933–944.
- [3] P. S. Lewis, British and Irish Hypertension Society’s Blood Pressure Measurement Working Party, Oscillometric measurement of blood pressure: a simplified explanation. a technical note on behalf of the british and irish hypertension society, *Journal of human hypertension* 33 (5) (2019) 349–351.
- [4] R. Mukkamala, G. S. Stergiou, A. P. Avolio, Cuffless blood pressure measurement, *Annual Review of Biomedical Engineering* 24 (2022) 203–230.
- [5] K. Kario, S. Ito, H. Itoh, H. Rakugi, Y. Okuda, S. Yamakawa, Effect of esaxerenone on nocturnal blood pressure and natriuretic peptide in different dipping phenotypes, *Hypertension Research* 45 (1) (2022) 97–105.
- [6] J. Shao, P. Shi, S. Hu, Y. Liu, H. Yu, et al., An optimization study of estimating blood pressure models based on pulse arrival time for continuous monitoring, *Journal of Healthcare Engineering* 2020 (2020).
- [7] P. Yousefian, S. Shin, A. S. Mousavi, A. Tivay, C.-S. Kim, R. Mukkamala, D.-G. Jang, B. H. Ko, J. Lee, U.-K. Kwon, et al., Pulse transit time-pulse wave analysis fusion based on wearable wrist ballistocardiogram for cuff-less blood pressure trend tracking, *IEEE Access* 8 (2020) 138077–138087.
- [8] A. Esmaili, M. Kachuee, M. Shabany, Nonlinear cuffless blood pressure estimation of healthy subjects using pulse transit time and arrival time, *IEEE Transactions on Instrumentation and Measurement* 66 (12) (2017) 3299–3308.
- [9] A.-G. Pielmus, J. Muehlstef, E. Bresch, M. Glos, C. Jungen, S. Mieke, R. Orglmeister, A. Schulze, B. Stender, V. Voigt, et al., Surrogate based continuous noninvasive blood pressure measurement, *Biomedical Engineering/Biomedizinische Technik* 66 (3) (2021) 231–245.

- [10] L. Geddes, M. Voelz, C. Babbs, J. Bourland, W. Tacker, Pulse transit time as an indicator of arterial blood pressure, *psychophysiology* 18 (1) (1981) 71–74.
- [11] B. Mishra, N. Thakkar, Cuffless blood pressure monitoring using ptt and pwv methods, in: 2017 International Conference on Recent Innovations in Signal processing and Embedded Systems (RISE), IEEE, 2017, pp. 395–401.
- [12] S. Baker, W. Xiang, I. Atkinson, A hybrid neural network for continuous and non-invasive estimation of blood pressure from raw electrocardiogram and photoplethysmogram waveforms, *Computer Methods and Programs in Biomedicine* 207 (2021) 106191.
- [13] B. Huang, W. Chen, C.-L. Lin, C.-F. Juang, J. Wang, Mlp-bp: A novel framework for cuffless blood pressure measurement with ppg and ecg signals based on mlp-mixer neural networks, *Biomedical Signal Processing and Control* 73 (2022) 103404.
- [14] T. Le, F. Ellington, T.-Y. Lee, K. Vo, M. Khine, S. K. Krishnan, N. Dutt, H. Cao, Continuous non-invasive blood pressure monitoring: a methodological review on measurement techniques, *IEEE Access* 8 (2020) 212478–212498.
- [15] K. Welykholowa, M. Hosanee, G. Chan, R. Cooper, P. A. Kyriacou, D. Zheng, J. Allen, D. Abbott, C. Menon, N. H. Lovell, et al., Multi-modal photoplethysmography-based approaches for improved detection of hypertension, *Journal of Clinical Medicine* 9 (4) (2020) 1203.
- [16] M. M. Bassiouni, I. Hegazy, N. Rizk, E.-S. A. El-Dahshan, A. M. Salem, Combination of ecg and ppg signals for smart healthcare systems: Techniques, applications, and challenges, in: 2021 Tenth International Conference on Intelligent Computing and Information Systems (ICICIS), IEEE, 2021, pp. 448–455.
- [17] P. C.-P. Chao, C.-C. Wu, D. H. Nguyen, B.-S. Nguyen, P.-C. Huang, V.-H. Le, The machine learnings leading the cuffless ppg blood pressure sensors into the next stage, *IEEE Sensors Journal* 21 (11) (2021) 12498–12510.

- [18] K. Qin, W. Huang, T. Zhang, Deep generative model with domain adversarial training for predicting arterial blood pressure waveform from photoplethysmogram signal, *Biomedical Signal Processing and Control* 70 (2021) 102972.
- [19] S. Mahmud, N. Ibtehaz, A. Khandakar, M. S. Rahman, A. J. Gonzales, T. Rahman, M. S. Hossain, M. S. A. Hossain, M. A. A. Faisal, F. F. Abir, et al., Nabnet: a nested attention-guided biconvlstm network for a robust prediction of blood pressure components from reconstructed arterial blood pressure waveforms using ppg and ecg signals, *Biomedical Signal Processing and Control* 79 (2023) 104247.
- [20] Z. Tian, A. Liu, G. Zhu, X. Chen, A paralleled cnn and transformer network for ppg-based cuff-less blood pressure estimation, *Biomedical Signal Processing and Control* 99 (2025) 106741.
- [21] R. Zhao, Y. Lu, L. Li, H. Ge, X. Fu, Amrunet: An attention-guided multiresunet for continuous noninvasive blood pressure estimation, in: 2024 International Joint Conference on Neural Networks (IJCNN), IEEE, 2024, pp. 1–8.
- [22] P. Guo, Y. Lu, J. Li, Y. Lv, J. Feng, Y. Liu, Cuffless blood pressure estimation model based on prior information of physiological data and lstm, *IEEE Sensors Journal* (2024).
- [23] J. Zhao, Q. Zhang, C. Qin, T. Lu, Z. Ning, Q. Guan, X. Ma, A lightweight convolutional neural network for personalized blood pressure estimation based on photoplethysmography, in: 2024 International Joint Conference on Neural Networks (IJCNN), IEEE, 2024, pp. 1–10.
- [24] D. Dai, Z. Ji, H. Wang, Non-invasive continuous blood pressure estimation from single-channel ppg based on a temporal convolutional network integrated with an attention mechanism, *Applied Sciences* 14 (14) (2024) 6061.
- [25] A. Hassani, A. H. Foruzan, Improved ppg-based estimation of the blood pressure using latent space features, *Signal, Image and Video Processing* 13 (2019) 1141–1147.
- [26] C. El Hajj, P. A. Kyriacou, Cuffless and continuous blood pressure estimation from ppg signals using recurrent neural networks, in: 2020 42nd

annual international conference of the IEEE engineering in medicine & biology society (EMBC), IEEE, 2020, pp. 4269–4272.

- [27] Y.-C. Hsu, Y.-H. Li, C.-C. Chang, L. N. Harfiya, Generalized deep neural network model for cuffless blood pressure estimation with photoplethysmogram signal only, *Sensors* 20 (19) (2020) 5668.
- [28] C. El-Hajj, P. A. Kyriacou, Cuffless blood pressure estimation from ppg signals and its derivatives using deep learning models, *Biomedical Signal Processing and Control* 70 (2021) 102984.
- [29] S. Gupta, A. Singh, A. Sharma, R. K. Tripathy, Higher order derivative-based integrated model for cuff-less blood pressure estimation and stratification using ppg signals, *IEEE Sensors Journal* 22 (22) (2022) 22030–22039.
- [30] M. Liu, L.-M. Po, H. Fu, Cuffless blood pressure estimation based on photoplethysmography signal and its second derivative, *International Journal of Computer Theory and Engineering* 9 (3) (2017) 202.
- [31] S. Rastegar, H. Gholam Hosseini, A. Lowe, Hybrid cnn-svr blood pressure estimation model using ecg and ppg signals, *Sensors* 23 (3) (2023) 1259.
- [32] A. Paviglianiti, V. Randazzo, S. Villata, G. Cirrincione, E. Pasero, A comparison of deep learning techniques for arterial blood pressure prediction, *Cognitive Computation* 14 (5) (2022) 1689–1710.
- [33] C. El-Hajj, P. A. Kyriacou, Deep learning models for cuffless blood pressure monitoring from ppg signals using attention mechanism, *Biomedical Signal Processing and Control* 65 (2021) 102301.
- [34] C. Ma, P. Zhang, F. Song, Y. Sun, G. Fan, T. Zhang, Y. Feng, G. Zhang, Kd-informer: Cuff-less continuous blood pressure waveform estimation approach based on single photoplethysmography, *IEEE Journal of Biomedical and Health Informatics* (2022).
- [35] S. Huang, R. Jafari, B. J. Mortazavi, Arterialnet: Arterial blood pressure reconstruction, in: 2023 IEEE EMBS International Conference on Biomedical and Health Informatics (BHI), IEEE, 2023, pp. 1–4.

- [36] C. Ma, P. Zhang, H. Zhang, Z. Liu, F. Song, Y. He, G. Zhang, Stp: Self-supervised transfer learning based on transformer for noninvasive blood pressure estimation using photoplethysmography, *Expert Systems with Applications* (2024) 123809.
- [37] M. W. Nawaz, M. A. Tahir, A. Mehmood, M. M. U. Rahman, K. Riaz, Q. H. Abbasi, Cuff-less arterial blood pressure waveform synthesis from single-site ppg using transformer & frequency-domain learning, *arXiv preprint arXiv:2401.05452* (2024).
- [38] A. Reiss, I. Indlekofer, P. Schmidt, PPG-DaLiA, *UCI Machine Learning Repository*, DOI: <https://doi.org/10.24432/C53890> (2019).
- [39] W. Wang, P. Mohseni, K. L. Kilgore, L. Najafizadeh, Cuff-less blood pressure estimation from photoplethysmography via visibility graph and transfer learning, *IEEE Journal of Biomedical and Health Informatics* 26 (5) (2021) 2075–2085.
- [40] A. Johnson, L. Bulgarelli, T. Pollard, S. Horng, L. A. Celi, R. Mark, Mimic-iv, PhysioNet. Available online at: <https://physionet.org/content/mimic-iv-ed/2.0/> (accessed August, 2023) (2020).
- [41] B. Moody, S. Hao, B. Gow, T. Pollard, W. Zong, R. Mark, Mimic-iv waveform database (version 0.1.0), <https://physionet.org/content/mimic4wdb/0.1.0/> (2022).
- [42] A. Tazarv, M. Levorato, A deep learning approach to predict blood pressure from ppg signals, in: 2021 43rd Annual International Conference of the IEEE Engineering in Medicine & Biology Society (EMBC), IEEE, 2021, pp. 1296–1299.
- [43] G. Slapničar, N. Mlakar, M. Luštrek, Blood pressure estimation from photoplethysmogram using a spectro-temporal deep neural network, *Sensors* 19 (15) (2019) 3420.
- [44] K. S. Kalyan, S. Sangeetha, Secnlp: A survey of embeddings in clinical natural language processing, *Journal of biomedical informatics* 101 (2020) 103323.

- [45] A. Vaswani, N. Shazeer, N. Parmar, J. Uszkoreit, L. Jones, A. N. Gomez, L. Kaiser, I. Polosukhin, Attention is all you need, *Advances in neural information processing systems* 30 (2017).
- [46] F. Schrumpf, P. Frenzel, C. Aust, G. Osterhoff, M. Fuchs, Assessment of non-invasive blood pressure prediction from ppg and rppg signals using deep learning, *Sensors* 21 (18) (2021) 6022.
- [47] N. Ibtehaz, S. Mahmud, M. E. Chowdhury, A. Khandakar, M. Salman Khan, M. A. Ayari, A. M. Tahir, M. S. Rahman, Ppg2abp: Translating photoplethysmogram (ppg) signals to arterial blood pressure (abp) waveforms, *Bioengineering* 9 (11) (2022) 692.
- [48] G. Slapničar, N. Mlakar, M. Luštrek, Blood pressure estimation from photoplethysmogram using a spectro-temporal deep neural network, *Sensors* 19 (15) (2019) 3420.
- [49] A. B. Malayeri, M. B. Khodabakhshi, Concatenated convolutional neural network model for cuffless blood pressure estimation using fuzzy recurrence properties of photoplethysmogram signals, *Scientific Reports* 12 (1) (2022) 6633.
- [50] F. Wu, A. Fan, A. Baevski, Y. N. Dauphin, M. Auli, Pay less attention with lightweight and dynamic convolutions, *arXiv preprint arXiv:1901.10430* (2019).
- [51] L. Jiang, X. Li, L. Wu, Y. Li, Bearing fault diagnosis method based on a multi-head graph attention network, *Measurement Science and Technology* 33 (7) (2022) 075012.
- [52] S.-J. Bu, S.-B. Cho, Time series forecasting with multi-headed attention-based deep learning for residential energy consumption, *Energies* 13 (18) (2020) 4722.
- [53] A. Nicolson, K. K. Paliwal, Masked multi-head self-attention for causal speech enhancement, *Speech Communication* 125 (2020) 80–96.
- [54] Z. Chen, E. Jiaze, X. Zhang, H. Sheng, X. Cheng, Multi-task time series forecasting with shared attention, in: 2020 International Conference on Data Mining Workshops (ICDMW), IEEE, 2020, pp. 917–925.

- [55] S. Reza, M. C. Ferreira, J. J. Machado, J. M. R. Tavares, A multi-head attention-based transformer model for traffic flow forecasting with a comparative analysis to recurrent neural networks, *Expert Systems with Applications* 202 (2022) 117275.
- [56] M. Blohm, G. Jagfeld, E. Sood, X. Yu, N. T. Vu, Comparing attention-based convolutional and recurrent neural networks: Success and limitations in machine reading comprehension, *arXiv preprint arXiv:1808.08744* (2018).
- [57] Y. Li, M. Du, S. He, Attention-based sequence-to-sequence model for time series imputation, *Entropy* 24 (12) (2022) 1798.
- [58] P. Niu, T. Zhou, X. Wang, L. Sun, R. Jin, Attention as robust representation for time series forecasting, *arXiv preprint arXiv:2402.05370* (2024).
- [59] A. Li, F. Xiao, C. Zhang, C. Fan, Attention-based interpretable neural network for building cooling load prediction, *Applied Energy* 299 (2021) 117238.
- [60] S. Ahmed, I. E. Nielsen, A. Tripathi, S. Siddiqui, G. Rasool, R. P. Ramachandran, Transformers in time-series analysis: A tutorial, *arXiv preprint arXiv:2205.01138* (2022).
- [61] H. Chen, L. Lyu, Z. Zeng, Y. Jin, Y. Zhang, Beat-to-beat continuous blood pressure estimation with optimal feature set of ppg and ecg signals using deep recurrent neural networks, *Vessel Plus* 7 (21) (2023).
- [62] H. Samimi, H. R. Dajani, A ppg-based calibration-free cuffless blood pressure estimation method using cardiovascular dynamics, *Sensors* 23 (8) (2023) 4145.
- [63] N. Q. Mahardika T, Y. N. Fuadah, D. U. Jeong, K. M. Lim, Ppg signals-based blood-pressure estimation using grid search in hyperparameter optimization of cnn-lstm, *Diagnostics* 13 (15) (2023) 2566.
- [64] Y. Chu, K. Tang, Y.-C. Hsu, T. Huang, D. Wang, W. Li, S. I. Savitz, X. Jiang, S. Shams, Non-invasive arterial blood pressure measurement and spo2 estimation using ppg signal: A deep learning framework, *BMC Medical Informatics and Decision Making* 23 (1) (2023) 131.

- [65] Y. Zhang, Z. Feng, A svm method for continuous blood pressure estimation from a ppg signal, in: Proceedings of the 9th international conference on machine learning and computing, 2017, pp. 128–132.
- [66] R. He, Z.-P. Huang, L.-Y. Ji, J.-K. Wu, H. Li, Z.-Q. Zhang, Beat-to-beat ambulatory blood pressure estimation based on random forest, in: 2016 IEEE 13th international conference on wearable and implantable body sensor networks (BSN), IEEE, 2016, pp. 194–198.
- [67] X. Che, M. Li, W. Kang, F. Lai, J. Wang, Continuous blood pressure estimation from two-channel ppg parameters by xgboost, in: 2019 IEEE International Conference on Robotics and Biomimetics (ROBIO), IEEE, 2019, pp. 2707–2712.